Research Article | Vol. 29, No. 9 / 26 April 2021 / Optics Express 13193
Optics EXPRESS

Controlled single-mode emission in quantum dot micro-lasers

SI ZHU,[1] XIANG MA,[2] CAN LIU,[2] WEI LUO,[1] JIA LIU,[2] BEI SHI,[1] WEIHUA GUO,[2,3] AND KEI MAY LAU[1,4]

[1]*Department of Electronic and Computer Engineering, Hong Kong University of Science and Technology, Clear Water Bay, Kowloon, Hong Kong*
[2]*Wuhan National Laboratory for Optoelectronics and the School of Optical and Electronic Information, Huazhong University of Science and Technology, Wuhan, China*
[3]*guow@hust.edu.cn*
[4]*eekmlau@ust.hk*

Abstract: In this paper, we demonstrate an efficient and easy fabrication method for whispering-gallery-mode (WGM) manipulation and report the first electrically driven single-mode quantum dot micro-ring (QDMR) lasers. Using self-assembled InAs/InAlGaAs QD active layers with deeply etched azimuthal gratings, continuous-wave (CW) lasing with controllable single-mode emission wavelengths covering 1300 nm to 1370 nm has been achieved. A record-high side-mode-suppression-ratio (SMSR) value of 49 dB is obtained. These QDMR lasers exhibit excellent single-mode lasing stabilities over the current and temperature tuning range with a thermal tunability of 0.092 nm/°C. The concept is applicable to other wavelength bands depending on the gain spectrum, demonstrating a feasible solution in realizing energy-efficient and densely integrated photonic building blocks.

1. Introduction

To satisfy the demand of rapidly growing data traffic in optical communications, the dimension and power dissipation of components in photonic integrated circuits (PICs) need to be significantly reduced [1,2]. One prerequisite enabling cost-effective scaling with increased chip density is to develop high performance micro-lasers with reliable monochromaticity. Featured with high-quality (Q) cavities and small mode volume, WGM micro-lasers are always alluring for practical low-power-consumption optical interconnects and dense photonic integration. To maintain feasible output powers and efficient current injection with minimum heat generation, the practical radius of a WGM micro-laser is usually on the order of tens of microns. In such a cavity, closely spaced high-Q WGMs overlapping with the gain spectrum generally results in chaotical multi-mode lasing and unstable mode hopping [3–6]. Even though several methods have been explored towards higher monochromaticity [7–13], so far the device performances are still limited to optical/pulsed electrical pumping with low SMSR values (10 dB ~ 36 dB). Furthermore, no studies on the stabilities of such single-mode operation in micro-lasers have ever been reported.

To significantly improve device performances, efforts should be devoted to both improved WGMs engineering and employing low-dimensional quantum structures as the gain material. The strategy proposed and implemented in this paper is to manufacture periodically structured azimuthal gratings on the outer periphery of the active micro-ring resonator. We have recently demonstrated microcylinder surface emitting lasers using GaAs-based quantum-wells (QWs) incorporating similar gratings [14]. Theoretically, quantum-dots (QDs) are featured with strong three-dimensional carrier confinement, which is beneficial for defect immunity and minimum surface recombination [15,16]. Considering the high sensitivity of WGMs to the sidewall defects, incorporating QDs as the laser gain elements helps mitigate these adverse impacts which degrade

#421037 https://doi.org/10.1364/OE.421037
Journal © 2021 Received 1 Feb 2021; revised 29 Mar 2021; accepted 7 Apr 2021; published 14 Apr 2021

Optics EXPRESS

the laser performances. In this work, electrically-pumped QD micro-lasers with precise spectral control and excellent single-mode stability has been realized for the first time. The high SMSR value of 49 dB obtained is much higher than the values ever reported by using other approaches, and this result is even comparable to the state-of-the-art DFB lasers [17–19]. Controllable single-mode lasing covering a wide band of ~70 nm is achieved for these QDMR lasers, due to the strong mode securing across the broad gain spectrum of QDs. Moreover, stable single-mode operation is achieved while tuning injection currents and temperatures.

2. Design and fabrication

The epitaxial growth was performed in a metal-organic chemical vapor deposition (MOCVD) system with a horizontal reactor (Aix 200/4). Figure 1(a) depicts the schematic diagram of the as-grown QD laser structure. Seven layers of self-assembled InAs/InAlGaAs QDs as the gain material were sandwiched between $In_{0.6}Al_{0.3}Ga_{0.1}As$ separate confinement heterostructures (SCHs). 1.5-μm-thick p-InP cladding and 140 nm p-InGaAs contact layer were grown on top subsequently, fully isolating the optical mode from the thick p-metals. The morphology of the topmost QD layer grown for morphology observation is revealed by an atomic force microscopy (AFM) image in the inset of Fig. 1(b), from which the QD density is estimated to be ~4×10^{10} cm^{-2}. Room-temperature photoluminescence (RT-PL) from the QDs (indicated by the arrow in Fig. 1(a)) is shown in Fig. 1(b). The center wavelength is approximately 1.31 μm, pumped by a 514 nm CW laser source. The emission from InAs QDs surrounded by InAlGaAs matrix can be tailored to cover both O- and C-band by varying the Al composition in the InAlGaAs alloy [20–22]. This unique characteristic enables a broader wavelength tuning range for the InAs/InAlGaAs QD system, compared to InAs/GaAs QD.

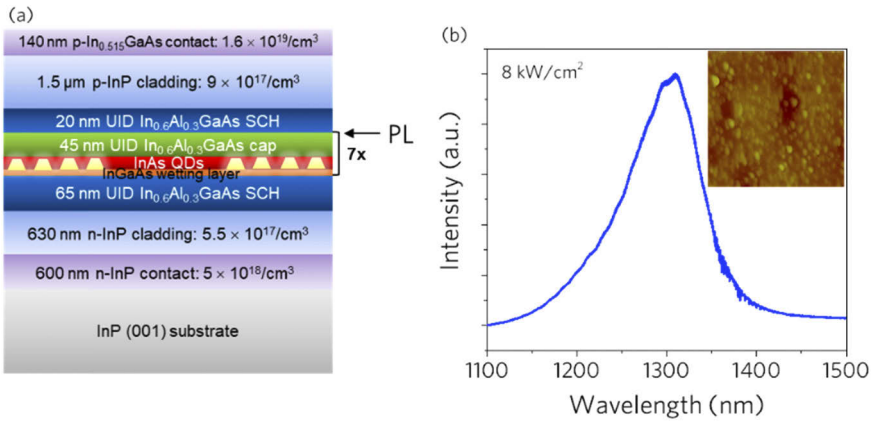

Fig. 1. (a) Schematic of the QD laser structure; (b) RT-PL spectrum pumped by 514 nm laser. Insert: 1 μm ×1 μm AFM image of the top-most QD layer.

Device fabrication procedures are graphically illustrated in Fig. 2. After SiO_2 deposition, E-beam lithography (EBL) was performed patterning sets of triangular-shape gratings together with the micro-ring cavities. The number of grating periods is fixed to the azimuthal mode order of the resonance WGM at the chosen single frequency. In such a way, the grating behaves as a second-order grating [23,24]. The EBL patterns were then transferred through the Cr layer down to the SiO_2 hard masks by lift-off, followed by ICP etching subsequently. Afterwards, a $Cl_2/CH_4/H_2$-based ICP dry etching was carried out to recess ~4 μm into the laser structure. Figure 3(a) presents a scanning electron microscope (SEM) image of one exemplary device with a 15 μm outer ring radius and a 3 μm ring waveguide width after dry etching. The sidewall smoothness of the grating is critical to the device performance, as a corrugated sidewall within

Optics EXPRESS

the active region gives rise to extra scattering loss. With an optimized deep ICP process, smooth and steep grating sidewall can be obtained as revealed in Fig. 3(b), ensuring minimum scattering loss introduced to the selected lasing mode. Meanwhile, the strong-carrier-localization nature of QDs allows for a more forgiving fabrication process comparing to QWs.

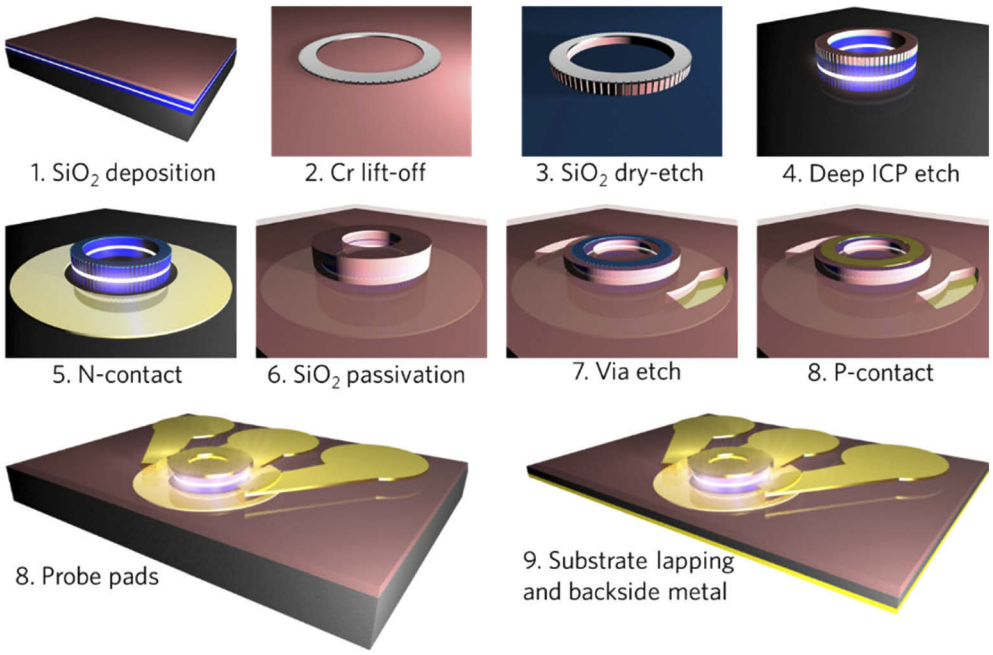

Fig. 2. Schematics of the process steps.

After deep-ICP etching, Ni/AuGe/Ni/Au metal stacks were evaporated on the n-InP surrounding the ring cavity. Afterwards, 800 nm of SiO_2 was deposited for isolation, followed by via openings and Pt/Ti/Pt/Au p-contact metal deposition. Ti/Au probe pads was then added. At last, to facilitate dicing and heat dissipation, the substrate was lapped and coated with the same n-metal stacks on the backside of the sample, which can also serve as an injection current contact. Figure 3(c) presents a top-view SEM image of an as-fabricated device. And a tilled zoom-in view of the grating-assisted cavity is presented in Fig. 3(d).

To illustrate and verify the working principle and effectiveness of these peripheral azimuthal gratings on single-mode selection, numerical simulations were performed based on the finite-difference time-domain (FDTD) method. Azimuthal mode order m = 84 for WGMs at 1.33 μm is selected for a microring cavity with an outer radius of 6 μm in the simulation. Quality factors (Q) for WGMs with different azimuthal mode numbers in the vicinity of m = 84 are calculated in Fig. 4(a) using the Padé approximation [25]. In the case of an ordinary microring laser where no gratings are applied (N = 0, N stands for the number of grating periods), all $TE_{m,0}$ modes share high Q-factors equally, leading to multi-mode lasing when these modes overlap with the gain spectrum. In the simulation, the degenerate clock-wise and counter-clock-wise traveling WGMs at each resonance frequency can be re-recognized as symmetric (sym.) and asymmetric (asym.) modes relative to a manually defined symmetry plane on the standing-wave basis, respectively [26]. When gratings with periods N = m = 84 are applied to the cavity periphery, only the symmetric mode with m = N maintains the highest Q factor on the order of 10^6. In sharp contrast, the Q factors of other modes are significantly diminished by three orders of magnitude due to strong perturbation interactions with the grating. This interaction introduces massive

Optics EXPRESS

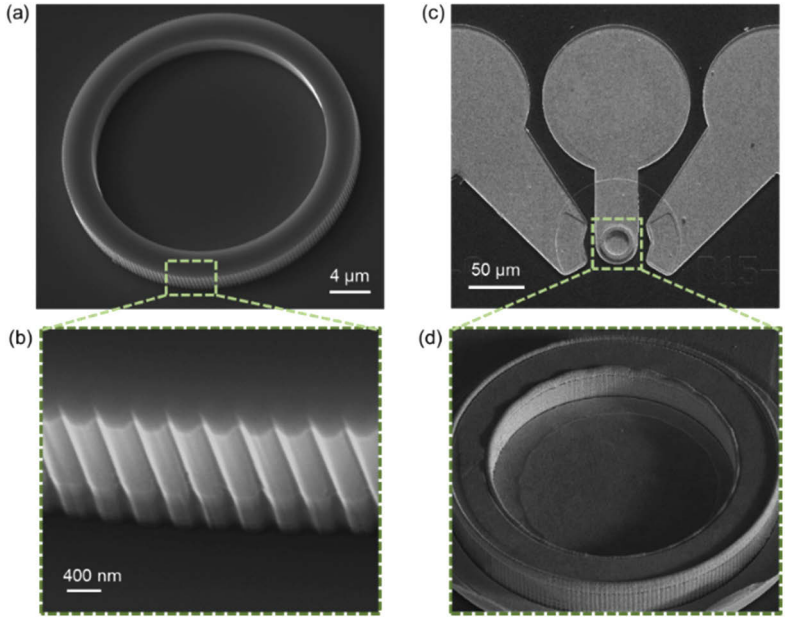

Fig. 3. SEM images of (a) the micro-ring cavity with 15 μm outer radius after deep ICP etch, (b) a zoom-in image of the peripheral gratings, (c) top-view of the as-fabricated device, and (d) close-up view of the laser cavity after all process steps.

radiation loss on the order of 10^2 cm^{-1} to these unselected modes, as illustrated in Fig. 4(b). In this way, the WGM with the azimuthal order m = N will stand out and achieve single-wavelength lasing. Figures 4(c) and 4(d) present the electric field ($|E|$) distributions of the two degenerate WGMs when m = N, indicating the locations of the field nodes and antinodes with respect to the

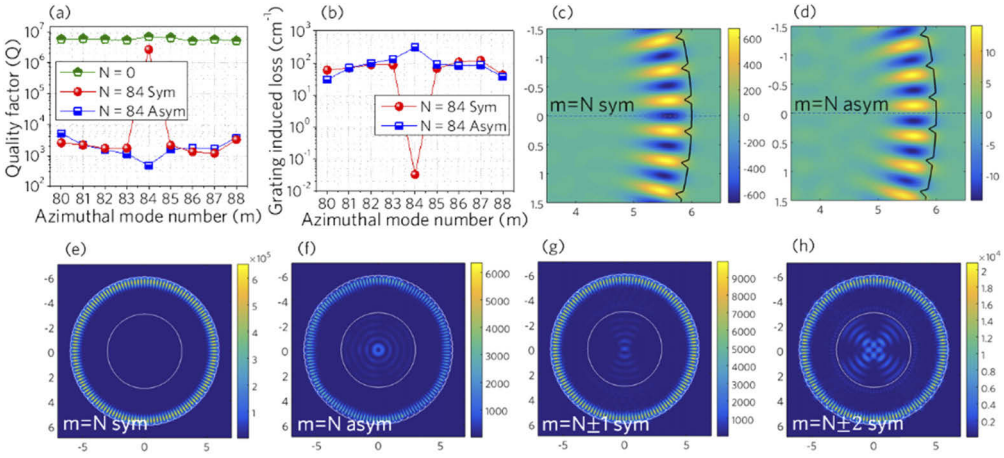

Fig. 4. FDTD simulation results illustrating the mode selection. N denotes the number of grating periods. m is the azimuthal order of the first radial order WGMs. (a) Simulated Q-factor and (b) grating induced loss as a function of m when N = 84 is applied to a 6-μm-radius ring cavity. Electrical field distribution of the degenerate (c), (e) symmetrical mode and (d), (f) asymmetrical mode when m = N, and the symmetrical mode when (g) m = N ± 1, and (h) m = N ± 2.

Optics EXPRESS

grating notches. The complete $|E|$ distributions for fundamental WGMs in the cases of m = N, m = N ± 1 and m = N ± 2 are shown in Figs. 4(e)–4(h). Interestingly, the radiation patterns exhibit a dominant azimuthal dependence on the order (m – N). The m = N symmetric mode radiates significantly less than others, manifesting the lowest radiation loss. Once the mechanism of these second-order azimuthal gratings is understood, the same idea can be transplanted to any wavelength band as long as the corresponding lasing mode is determined.

3. Results and discussion

3.1. Room-temperature continuous-wave lasing characteristics

For light-current (L-I) characterization, the devices were placed on a copper stage and subjected to CW current injections. The output power was collected by a Ge large-area photodetector from the top of the device. Figures 5(a) and 5(b) present L-I curves obtained from randomly selected QDMR lasers on the chip without and with gratings. The outer radius of the QDMR laser is 15 μm in both cases. As shown in Fig. 5(a), chaotic kinks exist on all L-I curves for ordinary QDMR lasers, indicating power fluctuations due to indiscriminate multi-mode lasing and mode hopping [27]. The lasing thresholds demonstrate a good consistency with an average lasing threshold of 10 mA.

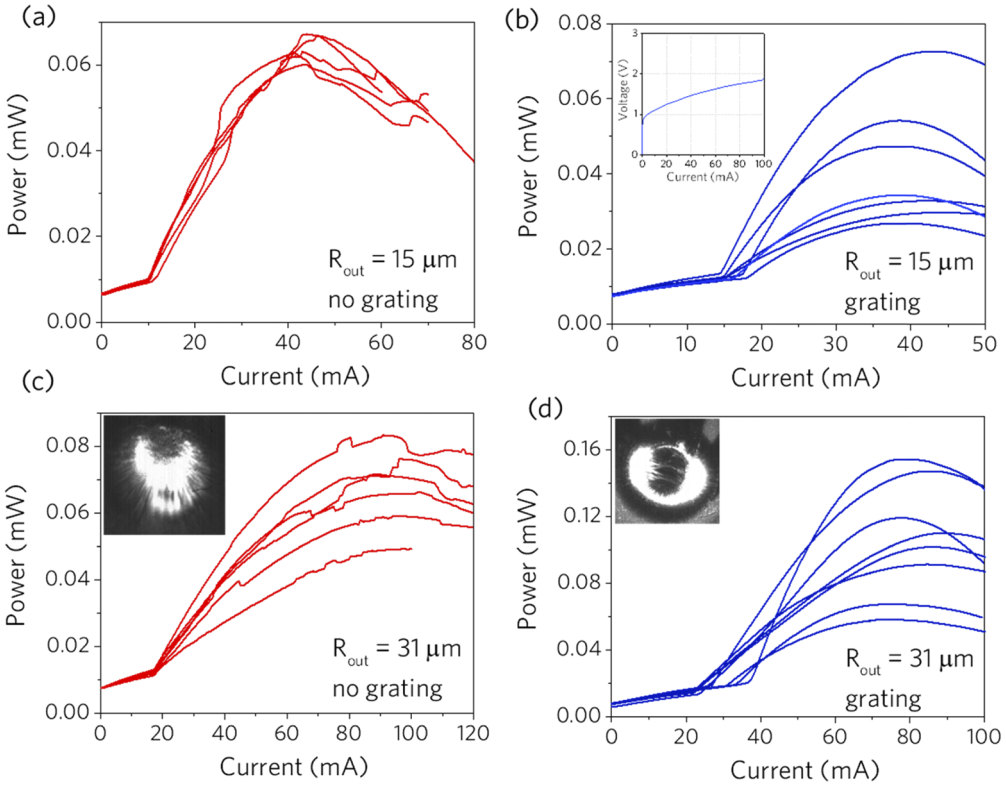

Fig. 5. Statistical L-I curves for R_{out} = 15 μm QD micro-ring lasers with (a) multi-mode lasing when no gratings applied, and (b) single-mode lasing with different grating designs. Insert: I-V curve; (c) Statistical L-I curves for R_{out} = 31 μm QD micro-ring lasers with (c) no gratings, and (d) gratings applied. Insets: near-field patterns collected from the top of each device.

Optics EXPRESS

In Fig. 5(b), all QDMR lasers with azimuthal gratings exhibit clean L-I characteristics, demonstrating excellent and stable single-mode lasing behavior from the onset of lasing till bend-over. The inset of Fig. 5(b) shows a representative I-V curve for the device. The series resistance can be extracted to be $R_s = 9\ \Omega$, which is crucial to minimize the heat generation and contributes to minor threshold increase at elevated operation temperatures. Measured devices were fabricated with different grating designs, either using different grating parameters or selecting lasing wavelengths that detunes differently from the gain peak, resulting in the threshold variation in Fig. 5(b). The influence of grating parameters and wavelength detuning will be further discussed in Section 3.2. This also leads to a slightly higher average lasing threshold (~ 15 mA) compared to that of the lasers without gratings. Additional scattering losses on the selected lasing mode with deeply etched sidewall gratings during the fabrication process also accounts for the threshold increase. The threshold discrepancy before and after adding the grating structure is expected to be much larger when other active media (i.e. quantum-wells) were used, since the WGMs are extremely sensitive to the sidewall smoothness of cavities, especially for device with small radius. The utilization of QDs as the gain elements already minimizes this threshold difference, owing to the higher immunity to the sidewall imperfection due to the strong carrier localization.

Remarkably, these gratings not only work well for the lasers with 15 μm radius but are also highly effective for larger device with 31 μm outer radius possessing more compact high-Q modes (FSR ≈ 3 nm) and higher emission power. Figures 5(c) and 5(d) show statistical L-I curves obtained from QDMR lasers without and with gratings with $R_{out} = 31$ um, from which the effectiveness of the azimuthal gratings is obvious. The inserts in Figs. 5(c) and 5(d) display their near-field patterns, respectively. The optical field of the ordinary micro-ring laser scatters in all directions, while the side scattering for lasers with gratings is suppressed and most of the optical field is scattered upwards. The enhanced vertical emission is further supported by the higher output power collected from the device top for QDMR lasers with azimuthal gratings (Fig. 5(d)). This is because the first order radiate direction of second-order gratings is perpendicular to the grating plane. This observation also demonstrates potentials for surface-emitting lasers [28] and beneficial when bonded to SOI wafer facilitating downwards coupling to Si waveguide [29].

Lasing spectra at progressively increased CW current injections for different devices without and with gratings are compared in Figs. 6(a)–6(c). Multi-mode lasing of adjacent WGMs around the gain peak is observed for ordinary micro-ring lasers without wavelength-selecting methods in Fig. 6(a). The free spectral range (FSR) for a 15-μm-radius ring is estimated to be around 5.5 nm ($FSR = \frac{\lambda^2}{2\pi n_g R_0}$), agreeing with the measured lasing peaks. Modes hopping to longer wavelengths are noticed with increasing current, which arises from the mode competition when the gain peak red shifts. Compared to the uncontrollable multi-mode lasing behavior, lasers with azimuthal gratings demonstrate exceptional current-dependent single-mode lasing stability. The lasing spectra shown in Fig. 6(d) are obtained from a 15 μm-radius micro-ring laser selecting the m = 217 mode. Stable single-mode lasing maintains a high SMSR around 40 dB from 20 mA to 50 mA with a current tuning of 0.12 nm/mA. Figure 6(c) presents the spectra for the device with 31 μm radius selecting m = 454 lasing mode at 1354 nm. A SMSR value as high as 49 dB can be achieved, which compares favorably to commercial DFB lasers.

By applying gratings with different periods, lasing at different wavelengths can be achieved. Benefiting from the broad gain spectrum of the QDs, steady single-mode lasing with SMSR ranging from ~35 dB to ~45 dB were measured from nine 15-μm-radius lasers with different grating periods, ranging from 1300 nm to 1370 nm (Figs. 6(d) and 6(e)). It should be mentioned that the band coverage can be wider, if the azimuthal WGM order larger than m = 225 or smaller than m = 213 were chosen in the initial layout design.

Optics EXPRESS

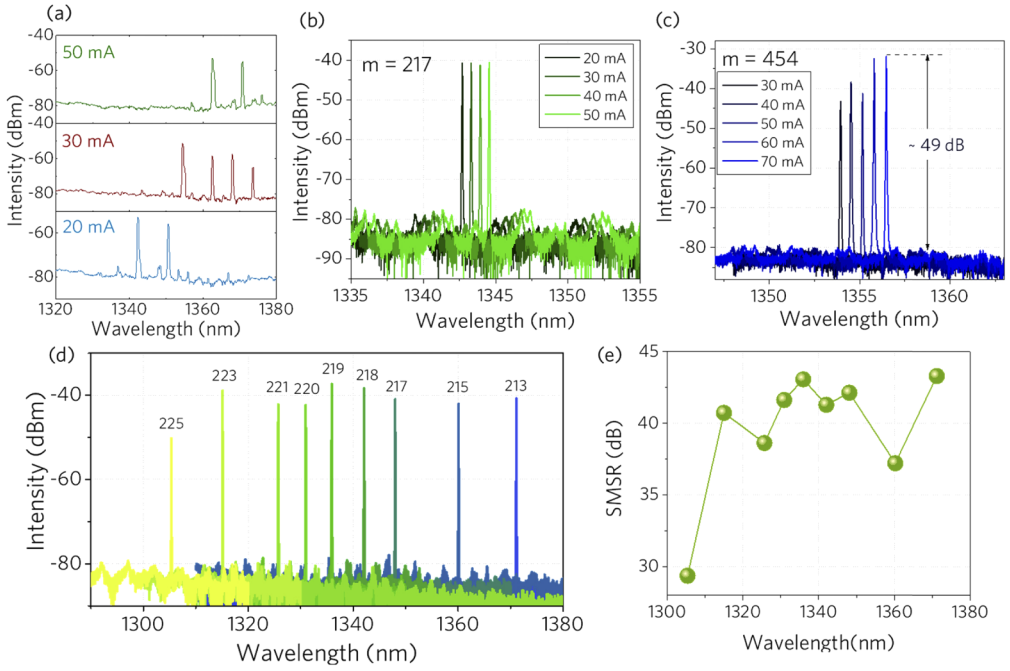

Fig. 6. (a) Multi-mode lasing spectra at different injection currents for an ordinary QDMR laser (no wavelength-selecting methods applied), and the outer radius is 15 μm; (b) Single-mode lasing spectra at various currents for the QDMR lasers with azimuthal gratings selecting m = 217 mode around 1343 nm (R_{out}=15 μm), and (c) m=454 mode around 1354 nm (R_{out}=31 μm); (d) Superimposed single-mode lasing spectra and (e) SMSR measured from nine 15-μm-radius devices at different lasing wavelengths, corresponding to WGMs of m = 213 to 225.

3.2. *Influence of the grating parameters and QD gain*

The grating parameters, i.e. the duty cycle (a/b) and the notch depth (c) schematically illustrated in the insert of Fig. 7(a), can both affect the amount of losses introduced to the selected m = N mode, which contributes to slight threshold variations for devices with different grating designs. Meanwhile, as a result of the unequal overlapping of QD gain with each mode, lasing threshold for each designed wavelength can be divergent. Figure 7(a) summarizes the relationship between the single-mode lasing threshold and the selected wavelength/mode as well as grating parameters, for R_{out} = 31 μm QD micro-ring lasers. Four different a/b and c combinations are presented. On the one hand, smaller grating duty cycle and deeper notch result in stronger interactions with the WGMs. While on the other hand, stronger perturbation and more radiation loss introduced into the unselected modes provide stronger restraints for them to lase. Therefore, single-mode lasing can be achieved even when the selected wavelength deviates from the gain peak. However, due to fabrication imperfections, smaller grating duty cycle and deeper notch will also bring about a small amount of scattering loss to the m = N mode and slightly increase the lasing threshold.

The general trend of the single-mode lasing threshold as a function of the wavelength agrees with measured gain spectrum shown in Fig. 7(b). The gain spectrum is extracted from the amplified spontaneous emissions of Fabry-Perot lasers (1.5 mm in length) simultaneously fabricated on the same wafer. Devices selecting lasing mode around 1345 nm possess the lowest threshold current, which is close to the gain peak. Besides, the lasing threshold increases when the selected mode/wavelength deviates from the gain peak. It is noted that the gain spectrum is

Optics EXPRESS

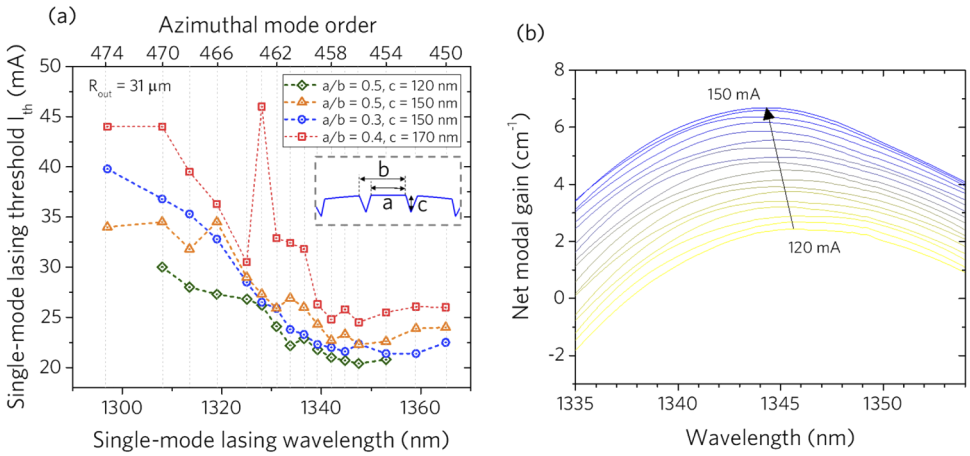

Fig. 7. (a) The relationship of single-mode lasing threshold with selected wavelength/mode and grating parameters for R_{out}=31 μm devices. Inset illustrates the grating parameters. a/b and c represent the duty cycle and notch depth respectively; (b) Gain spectra of the QD lasers.

several tens of nanometers longer than the PL peak shown in Fig. 1(b). This is because the lower energy states are inverted more easily due to their lower density of states and will thus have more gain compared to the higher energy states when pumping the laser. But since their density is lower, they also contribute less to the PL intensity [30,31].

3.3. *Thermal tuning capability*

These QDMR lasers have demonstrated superior single-mode lasing characteristics at room temperature. In practical applications, the chip temperature fluctuations could significantly affect the lasing behavior. Therefore, we further investigate the temperature-dependent lasing characteristics for these QDMR lasers. Figures 8(a) and 8(b) present two sets of L-I curves measured at various temperatures under CW current injections for ordinary micro-ring lasers without gratings and a single-mode laser with gratings selecting m = 218 mode, respectively. The difference between these two sets of L-I curves is conspicuous. As discussed above, the bumpy curves shown in Fig. 8(a) suggest the multi-mode lasing and mode hopping behavior, while smooth L-I curves are observed in Fig. 8(b), indicating a stable single-mode operation at increased temperatures. The characteristics temperature T_0 for these two lasers are extracted from the relationship $I(T)I(T) = \exp(T - TT)$, and presented in Figs. 8(c) and 8(d). The T_0 value is anticipated to be dramatically increased by p-type modulation doping [32]. Meanwhile, improved homogeneity of the as-grown InAs/InAlGaAs QDs will enlarge the energy state separation, which leads to a better temperature-dependent characteristic.

In addition, the multi-mode micro-lasers yield a higher operation temperature than the single-mode ones. Because the gain spectrum red shifts when temperature rises, the lasers without any mode restriction can hop to longer wavelengths to lase (Fig. 9(a)), while the lasers with gratings can only lase at the selected mode. Figure 9(b) shows the superimposition of two sets of lasing spectra measured from two 15-μm-radius lasers with the chosen WGM of m = 218 and m = 217 and lasing at around 1342 nm and 1347 nm, respectively. Steady single-mode lasing with a high SMSR around 45 dB is unveiled. When the chip temperature rises to higher than 35 °C, a gradual drop of SMSR can be observed due to a decreased optical efficiency. Note that our measurement could magnify this decrease because of the vibration of the fiber tip placed near the sample during heating. The single-mode lasing wavelength can be thermally tuned at

Optics EXPRESS

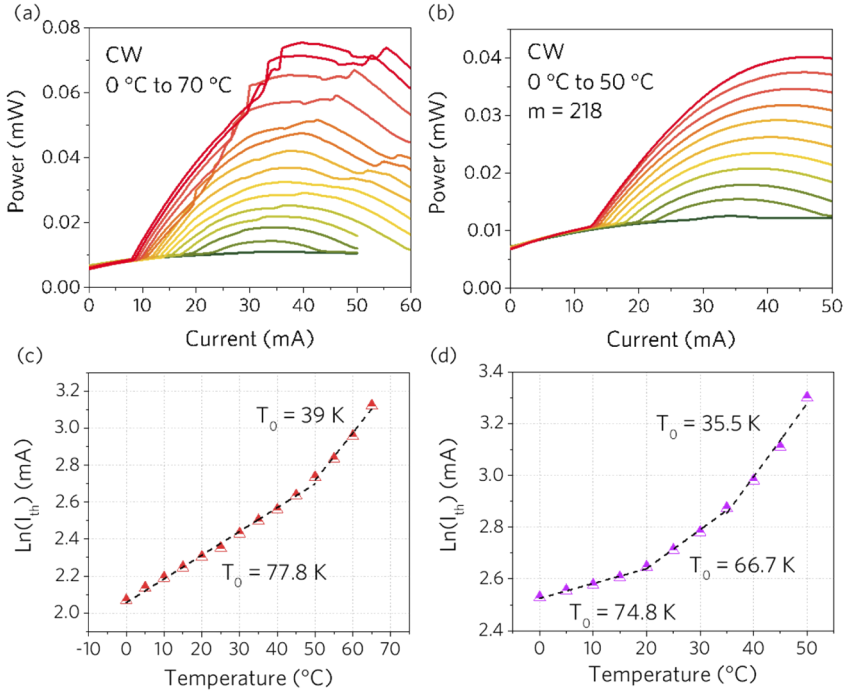

Fig. 8. L-I curves measured at various temperatures under CW pumping for QDMR lasers (a) without gratings, and (b) with gratings selecting m = 218 mode. The outer radius is 15 μm. (c) Relationship of the nature logarithm of lasing threshold current as a function of temperature for an ordinary QDMR laser with R_{out} = 15 μm and (d) single-mode QDMR laser with gratings selecting the m = 218 mode. The characteristic temperatures T_0 at different temperature ranges are extracted.

a coefficient of 0.092 nm/°C. With proper additional designs for on-chip thermal management [33,34], these lasers can have better thermal performances and be thermally tunable.

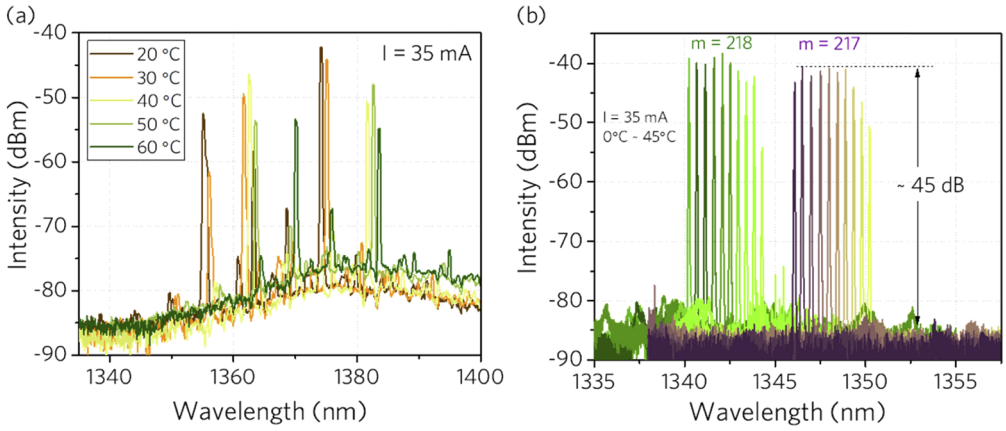

Fig. 9. (a) Multi-mode lasing spectra for an ordinary MRL at various temperatures; (b) Superimposition of single-mode lasing spectra at different temperatures measured from two R_{out} = 15 μm lasers selecting m = 218 and m = 217 modes.

Optics EXPRESS

4. Conclusion and outlook

In conclusion, utilizing QDs as gain medium and deeply etched peripheral azimuthal gratings, electrically-pumped CW micro-ring lasers are demonstrated for the first time, revealing excellent single-mode lasing behaviors. Experimental results show a controllable single-mode operation covering a ~70 nm lasing wavelength range with SMSR values maintained at around 40 dB. The highest SMSR of 49 dB is nearly two times higher than the values reported using other approaches to realize single-mode micro-lasers. There is still room for improvement in terms of the power consumption and device efficiency, which can be achieved by further enhancing the gain and internal quantum efficiency of the as-grown QDs, as well as efficiently extracting the unidirectional output power from the WGM lasers [35]. Comprehensive analysis on the influence of the grating parameters and the QD gain on the single-mode lasing thresholds as well as thermal tunability have been discussed, offering insights for improved device designs. These single-mode QDMR lasers advance the future in-plane integration in compact multi-channel transmitters.

Funding. Innovation Technology Fund of Hong Kong (ITS/273/16FP); National Natural Science Foundation of China (61675077, 61861136001, 61875066); Research Grants Council, University Grants Committee (16212115, 614813).

Acknowledgments. The authors thank Prof. Andrew Wing-On Poon, Dr. Quanan Chen, Ms. Chun Jiang, Mr. Gonghai Liu and Mr. Su Tan for helpful discussions.

Disclosures. The authors declare no conflicts of interest.

References

1. L. Thylén, S. He, L. Wosinski, and D. Dai, "The Moore's Law for photonic integrated circuits," J. Zhejiang Univ., Sci., A **7**(12), 1961–1967 (2006).
2. M. Smit, J. van der Tol, and M. Hill, "Moore's law in photonics," Laser Photonics Rev. **6**(1), 1–13 (2012).
3. M. T. Hill, S. Anantathanasarn, Y. Zhu, Y.-S. Oei, P. Van Veldhoven, M. Smit, and R. Notzel, "InAs–InP (1.55-μ m Region) Quantum-Dot Microring Lasers," IEEE Photonics Technol. Lett. **20**(6), 446–448 (2008).
4. S. McCall, A. Levi, R. Slusher, S. Pearton, and R. Logan, "Whispering-gallery mode microdisk lasers," Appl. Phys. Lett. **60**(3), 289–291 (1992).
5. G. Mezosi, M. J. Strain, S. Furst, and M. Sorel, "Bistable micro-ring lasers with compact footprint and high output efficiency," IEEE J. Quantum Electron. **48**(8), 1023–1030 (2012).
6. A. Bennecer, K. Williams, R. Penty, I. White, M. Hamacher, and H. Heidrich, "Directly modulated wavelength-multiplexed integrated microring laser array," IEEE Photonics Technol. Lett. **20**(16), 1411–1413 (2008).
7. A. Arbabi, S. M. Kamali, E. Arbabi, B. G. Griffin, and L. L. Goddard, "Grating integrated single mode microring laser," Opt. Express **23**(4), 5335–5347 (2015).
8. M. Fujita and T. Baba, "Microgear laser," Appl. Phys. Lett. **80**(12), 2051–2053 (2002).
9. W.-G. Yao, K.-M. Guan, Z.-N. Tian, J.-J. Xu, Q.-D. Chen, and H.-B. Sun, "Mode-selecting micrograting cavity laser," J. Lightwave Technol. **34**(17), 4143–4147 (2016).
10. W. Liu, M. Li, R. S. Guzzon, E. J. Norberg, J. S. Parker, M. Lu, L. A. Coldren, and J. Yao, "An integrated parity-time symmetric wavelength-tunable single-mode microring laser," Nat. Commun. **8**(1), 15389 (2017).
11. L. Feng, Z. J. Wong, R.-M. Ma, Y. Wang, and X. Zhang, "Single-mode laser by parity-time symmetry breaking," Science **346**(6212), 972–975 (2014).
12. H. Hodaei, M.-A. Miri, A. U. Hassan, W. E. Hayenga, M. Heinrich, D. N. Christodoulides, and M. Khajavikhan, "Single mode lasing in transversely multi-moded PT-symmetric microring resonators," Laser Photonics Rev. **10**(3), 494–499 (2016).
13. H. Hodaei, M.-A. Miri, M. Heinrich, D. N. Christodoulides, and M. Khajavikhan, "Parity-time–symmetric microring lasers," Science **346**(6212), 975–978 (2014).
14. X. Ma, Q. Chen, J. Liu, Y. Liu, W. Sun, G. Liu, C. Liu, Q. Lu, and W. Guo, "Demonstration of Low-Threshold and Directly Modulated Grating-Assisted Microcylinder Surface-Emitting Lasers," J. Lightwave Technol. **38**(17), 4772–4779 (2020).
15. S. A. Moore, L. O'Faolain, M. A. Cataluna, M. B. Flynn, M. V. Kotlyar, and T. F. Krauss, "Reduced surface sidewall recombination and diffusion in quantum-dot lasers," IEEE Photonics Technol. Lett. **18**(17), 1861–1863 (2006).
16. S. Zhu, B. Shi, Y. Wan, E. L. Hu, and K. M. Lau, "1.55 μm band low-threshold, continuous-wave lasing from InAs/InAlGaAs quantum dot microdisks," Opt. Lett. **42**(4), 679–682 (2017).
17. R. Millett, K. Dridi, A. Benhsaien, H. Schriemer, K. Hinzer, and T. Hall, "Fabrication-tolerant 1310 nm laterally coupled distributed feedback lasers with high side mode suppression ratios," Photonics Nanostructures: Fundam. Appl. **9**(2), 88–92 (2011).
18. K. Kudo, K. Yashiki, T. Sasaki, Y. Yokoyama, K. Hamamoto, T. Morimoto, and M. Yamaguchi, "1.55-μm wavelength-selectable microarray DFB-LD's with monolithically integrated MMI combiner, SOA, and EA-Modulator," IEEE Photonics Technol. Lett. **12**(3), 242–244 (2000).

Optics EXPRESS

19. J. S. Kim, J. H. Lee, S. U. Hong, H.-S. Kwack, B. S. Choi, and D. K. Oh, "InAs-InAlGaAs quantum dot DFB lasers based on InP [001]," IEEE Photonics Technol. Lett. **18**(4), 595–597 (2006).
20. S. Zhu, B. Shi, Q. Li, and K. M. Lau, "1.5 μ m quantum-dot diode lasers directly grown on CMOS-standard (001) silicon," Appl. Phys. Lett. **113**(22), 221103 (2018).
21. S. Zhu, B. Shi, and K. M. Lau, "Electrically pumped 1.5 μm InP-based quantum dot microring lasers directly grown on (001) Si," Opt. Lett. **44**(18), 4566–4569 (2019).
22. W. Luo, Y. Xue, B. Shi, S. Zhu, X. Dong, and K. M. Lau, "MOCVD growth of InP-based 1.3 μm quantum dash lasers on (001) Si," Appl. Phys. Lett. **116**(14), 142106 (2020).
23. R. Kazarinov and C. Henry, "Second-order distributed feedback lasers with mode selection provided by first-order radiation losses," IEEE J. Quantum Electron. **21**(2), 144–150 (1985).
24. W. Park and S. Seshadri, "Theory of the second-order reflection grating," J. Opt. Soc. Am. A **3**(10), 1632–1643 (1986).
25. W.-H. Guo, W.-J. Li, and Y.-Z. Huang, "Computation of resonant frequencies and quality factors of cavities by FDTD technique and Padé approximation," IEEE Microw. Wireless Compon. Lett. **11**(5), 223–225 (2001).
26. X. Ma, Q. Chen, Q. Lu, and W. Guo, "Grating-Assisted Microcylinder Surface-Emitting Laser," J. Lightwave Technol. **34**(21), 4999–5006 (2016).
27. L. A. Coldren, S. W. Corzine, and M. L. Mashanovitch, *Diode lasers and photonic integrated circuits*: John Wiley & Sons, 2012.
28. L. Mahler, A. Tredicucci, F. Beltram, C. Walther, J. Faist, H. E. Beere, and D. A. Ritchie, "High-power surface emission from terahertz distributed feedback lasers with a dual-slit unit cell," Appl. Phys. Lett. **96**(19), 191109 (2010).
29. C. Zhang, D. Liang, G. Kurczveil, A. Descos, and R. G. Beausoleil, "Hybrid quantum-dot microring laser on silicon," Optica **6**(9), 1145 (2019).
30. J. Buus, *Single frequency semiconductor lasers*: SPIE Press, 1991.
31. J. Hader, S. W. Koch, and J. V. Moloney, "Microscopic theory of gain and spontaneous emission in GaInNAs laser material," Solid-State Electron. **47**(3), 513–521 (2003).
32. A. Matsumoto, K. Akahane, T. Umezawa, and N. Yamamoto, "Extremely stable temperature characteristics of 1550-nm band, p-doped, highly stacked quantum-dot laser diodes," Jpn. J. Appl. Phys. **56**(4S), 04CH07 (2017).
33. D. Liang, X. Huang, G. Kurczveil, M. Fiorentino, and R. Beausoleil, "Integrated finely tunable microring laser on silicon," Nat. Photonics **10**(11), 719–722 (2016).
34. C. Zhang, D. Liang, G. Kurczveil, J. E. Bowers, and R. G. Beausoleil, "Thermal management of hybrid silicon ring lasers for high temperature operation," IEEE J. Sel. Top. Quantum Electron. **21**(6), 385–391 (2015).
35. X. F. Jiang, C. L. Zou, L. Wang, Q. Gong, and Y. F. Xiao, "Whispering-gallery microcavities with unidirectional laser emission," Laser Photonics Rev. **10**(1), 40–61 (2016).